Optimized Interferential Stimulation of Human Brains

Yu Huang[a,b], Abhishek Datta[b], Lucas C. Parra[a]

[a]*Department of Biomedical Engineering, City College of the City University of New York, New York, NY, USA, 10031*
[b]*Research & Development, Soterix Medical, Inc., New York, NY, USA, 10001*

Abstract

Interferential stimulation (IFS) has generated considerable interest recently because of its potential to achieve focal electrical stimulation in deep brain areas despite applying currents transcranially. Conventionally, IFS applies sinusoidal currents through two electrode pairs with close-by frequencies. Here we propose to use two arrays of scalp electrodes with current intensity through each electrode optimized to target a desired location in the brain. We formulate rigorous optimization criteria for IFS to achieve either maximal modulation depth or most focal stimulation. For max-modulation optimization we show analytically that the solution is the same for IFS as for conventional multi-electrode stimulation. We proof that the solution can be found directly from the forward model without the need for algorithmic optimization. For the max-focality criterion the solution requires numerical optimization. Once optimized, we find that IFS can achieve more focal modulation of stimulation intensity than conventional stimulation with a single frequency, both at the cortical surface and deep in the brain.

Keywords: transcranial electrical stimulation, interferential stimulation, mathematical optimization, computational models

1. Introduction

Transcranial electric stimulation (TES) delivers weak electric current ($\leq$ 2 mA) into the brain to modulate neural activities (Nitsche and Paulus, 2000). Research has shown that TES can improve performance in some learning tasks and has also shown promise as a therapy for a number of neurological disorders such as depression, fibromyalgia and stroke (Nitsche et al., 2003; Fregni et al., 2006; Bikson et al., 2008; Schlaug et al., 2008). Conventional TES uses two sponge-electrodes to deliver current to the scalp. Modeling studies suggest that electric fields generated with such an approach are diffuse in the brain and typically cannot reach deep targets in the brain (Datta et al., 2009). A number of investigators have advocated the use of several small "high-definition" electrodes to achieve more focal or more intense stimulation (Datta et al., 2009; Dmochowski et al., 2011). This multi-electrode approach is referred to as high-definition transcranial electric stimulation (HD-TES, Edwards et al., 2013), and can be combined with any desired stimulation waveform.

Recently Grossman et al. (2017) proposed to stimulate the brain with "interferential stimulation" (IFS), which is well known in physical therapy (Goats, 1990). IFS applies sinusoidal waveforms of similar frequency through two electrode pairs. The investigators suggest that interference of these two waveforms can result in modulation of oscillating fields deep inside the brain. The promise of non-invasive deep brain stimulation has caused considerable excitement

in the research community and in the news media (Dmochowski and Bikson, 2017; Shen, 2018). Our subsequent analysis of IFS suggests that it may not differ much from other multi-electrode methods in terms of intensity of stimulation (Huang and Parra, 2019). However, this conclusion is limited to the case of IFS using only two electrodes for each of the two currents. More recently researchers have turned to optimizing IFS in the hope that stimulation can be more focal in deep brain areas. A series of approaches have been propose, but all are limited in some respect. Rampersad et al. (2019) searches through a large number of montages with two pairs of electrodes, but does not systematically tackle the general problem of arrays. Cao and Grover (2019) suggests the use of arrays, but fails to take interference into account by optimizing each frequency separately. Xiao et al. (2019) also proposes multiple pairs of electrodes but does not systematically optimize how to place them and what current to use through each.

Here we present a mathematical formulation of the optimization of IFS, including for the case of more than two electrode pairs. This allows us to systematically optimize the location of electrodes and the strength of injected currents through each electrode. Fundamentally, this array version of IFS differs from HD-TES only in that IFS uses two sinusoidal frequencies, whereas HD-TES uses the same waveform in all electrodes of the array. We show mathematically, and confirm numerically, that maximal modulation of interfering waveforms can be simply obtained by maximizing intensity of conventional HD-TES. We also provide a mathematical proof that the solution of max-intensity stimulation can be obtained directly from the forward model for TES, as first proposed by Fernandez-Corazza et al. (2019). Motivated by Guler et al. (2016) and Fernandez-Corazza et al. (2019), we convert the computationally intractable max-focality optimization for IFS into a max-intensity problem with constraint on the energy in the non-target area. This non-convex optimization is treated as a goal attainment problem (Gembicki and Haimes, 1975) and then solved by sequential quadratic programming (Brayton et al., 1979). IFS optimization in terms of intensity and focality is evaluated on the MNI-152 head model (Grabner et al., 2006) and compared to HD-TES solutions. Results show that one can achieve improved focality of modulation in deep brain areas as compared to HD-TES. This opens the possibility for non-invasive focal deep brain stimulation in the future.

2. Methods

2.1. Mathematical formulation

The mathematical framework for optimizing arrays of electrodes for TES was first introduced by Dmochowski et al. (2011). An important conclusion of that work was that there is a fundamental trade-off between achieving intense stimulation on a desired target, versus achieving focally constrained stimulation at that location. Thus, a number of competing optimization criteria were proposed in that work. Since then additional criteria have been proposed that strike a different balance or improve on computational efficiency. The criterion we used here is heavily motivated by Guler et al. (2016) because their formulation readily extends to IFS. Importantly, we now realize that the formulation allows one to readily adjust the trade-off between intensity and focality of stimulation. Let us explain.

The goal of targeting is to find an optimal source distribution $\mathbf{s}$ across a set of candidate electrode locations on the scalp. With M locations this vector $\mathbf{s}$ has M dimensions, including one location reserved for the reference electrode. Since all currents entering the tissue must also exit, the sum of currents has to vanish, $\mathbf{1s} = 0$ (Here $\mathbf{1}$ is a M-dimensional row vector with all values

set to 1. The inner product with this vector executes a sum). The electric field generated in the tissue by this current distribution $\mathbf{s}$ on the scalp is given by:

$$\mathbf{E} = \mathbf{A}\mathbf{s}, \tag{1}$$

where $\mathbf{A}$ is the "forward model" for TES. Specifically, it is a matrix that quantifies in each column the electric field generated in the tissue when passing a unit current from one electrode to the reference electrode. If there are M electrode locations and N locations in the brain to be considered, then matrix $\mathbf{A}$ has M columns and $3N$ rows (one for each of the three directions of the field). The column corresponding to the reference electrode has all zero values as current enters and exits through the same electrode, i.e. no current flows through the tissue, and no field is generated.

One goal of the optimization may be to maximize the intensity of stimulation at the target in a desired direction:

$$\begin{aligned} \arg\max_{\mathbf{s}} \quad & \mathbf{e}^T\mathbf{A}\mathbf{s}. \\ \text{s.t. } & \mathbf{1}\mathbf{s} = 0 \end{aligned} \tag{2}$$

Here vector $\mathbf{e}$ is used to specify the desired field distribution and direction at the target. For example, the values of the vector $\mathbf{e}$ might be set to zero everywhere, except at the target location. If the desired target covers more than one location, then the non-zero values extend over all the corresponding locations. The specific values of $\mathbf{e}$ determine the desired orientation of the electric field.

At a minimum this optimization should be subject to the constraint that the total current injected shall not exceed a maximum value I_{max}, otherwise this might cause discomfort or irritation on the scalp. The total applied current is the sum of absolute current through all electrodes:

$$\mathbf{1}|\mathbf{s}| \leq 2I_{max}. \tag{3}$$

As the total current has to enter and exit the head it contributes to this sum twice, which explains the factor of 2 in the upper bound. In addition to this total current constraint, Guler et al. (2016) proposes to constrain the power of the electric field in brain areas outside the target region:

$$||\mathbf{\Gamma}\mathbf{A}\mathbf{s}||^2 \leq P_{max}. \tag{4}$$

The spatial selectivity for the non-target area is captured here by the diagonal matrix $\mathbf{\Gamma}$. The diagonal elements of this matrix are zero for the target region, and non-zero elsewhere. These non-zero values can additionally implement a relative weighting for different locations (say, to compensate for uneven sampling in the FEM mesh, or to emphasize some regions more than others, although we do not do this here).

A few comments are in order here:

As pointed out by Guler et al. (2016), this quadratic criterion can be evaluated efficiently as, $\mathbf{s}^T\mathbf{Q}\mathbf{s} \leq P_{max}$, which is fast to compute because, $\mathbf{Q} = \mathbf{A}^T\mathbf{\Gamma}^2\mathbf{A}$, is a compact $M \times M$ matrix.

Constraints (3) and (4) specify a convex feasibility region and thus the optimization of the linear criterion can be solved with convex programming (see Section 2.5). In fact, when only the linear constraint (3) is active the solution can be found without the need for numerical optimization at all. We provide a prescription for how to find these solutions, along with a proof in Section 2.3.

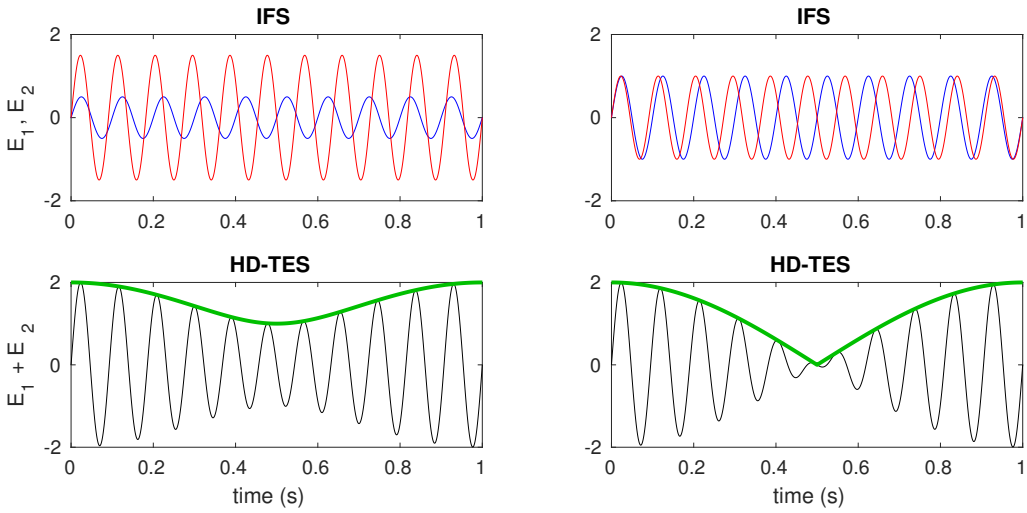

Figure 1: Modulation vs. Intensity: In IFS, stimulation is delivered as sinusoidal waveforms with close-by frequencies (top, red and blue). When added together they overlap to generate a modulated waveform referred to as the carrier (bottom, black). The envelope (green) of the modulated carrier waveform oscillates at the difference frequency, in this example $f_1 = 10, f_2 = 11, \Delta f = 1$ Hz. HD-TES can apply a single waveform of any shape, in particular, it can apply a modulated sinusoid (black). In the hypothetical example on the left the waveform has an intensity of 2 V/m and a modulation depth of 1 V/m, corresponding to 50% modulation. In the example on the right intensity and modulation depth are both 2 V/m, i.e. a modulation depth of 100%. HD-TES can always ensure a modulation depth of 100% so we treat intensity and modulation depth as equivalent. For IFS modulation depth can only be 100% when both fields at a given location have the same magnitude. In most locations fields will not be the same for both frequencies and modulation depth will be less than the intensity (as in the example on the left). The only way for both fields to be identical everywhere for IFS is for current amplitude to be identical for both frequencies in all electrodes.

The power constraint (4) can be used to titrate between maximally intense stimulation and maximally focal stimulation. Specifically, if P_{max} is set very high so as to not limit currents at all, then we are left only with the constraint (3) on current intensity. Criterion (2) subject to constraint (3) is the optimization proposed by Dmochowski et al. (2011) to achieve maximally intense stimulation. If, on the other hand, P_{max} is set to a very stringent value, then the constraint (4) dominates the maximization problem as shown by Guler et al. (2016). In that case we are left with criterion (2) subject to the power constraint (4). Fernandez-Corazza et al. (2019) show that this is equivalent to the least-squares criterion, which was introduced by Dmochowski et al. (2011) to achieve focal stimulation. The equivalence is only approximate, but becomes accurate if the target region is chosen to be small. In Section 3.1 we will show how intermediate values of P_{max} can move us between these two extremes of maximal intensity versus maximal focality.

Now we move on to the issue of optimizing IFS with electrode arrays.

2.2. *Optimization of intensity in interferential stimulation*

In inferential stimulation two fields oscillating sinusoidally at similar frequencies interfere to cause an amplitude modulation of the oscillating waveform. This leads to two different quantities: modulation depth and intensity of the carrier signal (Figure 1). One can always use a 100% amplitude-modulated current in HD-TES, meaning modulation depth is the same as signal intensity. On the other hand, modulation depth is weaker than signal intensity in IFS if the two

interfering currents have different amplitudes. We use the terms "modulation depth" and "intensity" interchangeably in this paper but we only optimize the modulation depth for both HD-TES and IFS (see Figures 3, 4 and 5 for the differences).

For IFS, if the electric field for one frequency is $\mathbf{E}_1$ and for the other frequency $\mathbf{E}_2$ then the modulation depth of the interfering fields is $2\min(|\mathbf{E_1}|, |\mathbf{E_2}|)$ (Huang and Parra, 2019). Let's assume that these two fields are generated by the current distributions $\mathbf{s}_1$ and $\mathbf{s}_2$, each oscillating at their own frequency. To maximize modulation depth at a location specified by vector $\mathbf{e}$, we propose the following criterion:

$$\begin{aligned} \underset{\mathbf{s}_1, \mathbf{s}_2}{\arg\max} \quad & 2\min(|\mathbf{e^T A s_1}|, |\mathbf{e^T A s_2}|)\,. \\ \text{s.t. } \mathbf{1s}_1 = 0, \mathbf{1s}_2 &= 0 \end{aligned} \tag{5}$$

The vectors $\mathbf{s}_1$ and $\mathbf{s}_2$ are both of length M. The zero sum constraints are needed to maintain physical feasibility. The vectors quantify currents in the same set of electrodes. Thus, each single electrode has the freedom to pass current at two different frequencies and intensities added together. This generalizes the conventional IFS approach (Grossman et al., 2017) in that each frequency is now applied to potentially more than one electrode pair. It is also more flexible than recent efforts to target IFS with multiple pairs as they are limited to applying only one oscillating frequency at each pair (Rampersad et al., 2019; Cao and Grover, 2019). In contrast, here each electrode can apply the sum of two oscillating currents, and thus we can variably distributed the two frequencies over all electrodes in the array.

For the sake of safety and comfort we again limit the total applied current to a maximum value:

$$\mathbf{1}|\mathbf{s}_1| \leq I_{max},\ \mathbf{1}|\mathbf{s}_2| \leq I_{max}. \tag{6}$$

Note that the optimization criterion (5) is bounded from above:

$$2\min(|\mathbf{E}_1|, |\mathbf{E}_2|) \leq |\mathbf{E}_1| + |\mathbf{E}_2| \tag{7}$$

and the equality holds, if and only if $|\mathbf{E}_1| = |\mathbf{E}_2|$. This implies that no matter what choice one makes for $\mathbf{s}_1$, the criterion (5) will always be maximal for $\mathbf{s}_2 = \mathbf{s}_1$ as then $|\mathbf{E}_1| = |\mathbf{E}_2|$. In other words, we can equivalently optimize for a single $\mathbf{s} = \mathbf{s}_1 = \mathbf{s}_2$ (subject to the same set of constraint):

$$\underset{\mathbf{s}_1, \mathbf{s}_2}{\arg\max}\ 2\min(|\mathbf{e}^T\mathbf{A}\mathbf{s}_1|, |\mathbf{e}^T\mathbf{A}\mathbf{s}_2|) = \underset{\mathbf{s}}{\arg\max}\ 2\mathbf{e}^T\mathbf{A}\mathbf{s}\,. \tag{8}$$

This criterion (8) is the same maximum-intensity criterion as (2), which we used for HD-TES. What does it mean that currents through electrodes are the same for both frequencies? It simply means that each electrode is passing the same amplitude-modulated waveform (with 100% modulation depth) with magnitude and sign as defined by $\mathbf{s}$. Therefore, to optimize the modulation depth of IFS one simply needs to "fuse" the two current sources. In short, the largest modulation depth of IFS will be achieved with the max-intensity solution of HD-TES. In Section 3.2 we provide numerical confirmation for this theoretical result, namely, that the maximum intensity criterion gives the same result for IFS and HD-TES.

2.3. Closed form solution for max-intensity optimization

Let's consider now the maximum-intensity problem of HD-TES as specified by (2) subject to (3). This is a linear criterion with a linear constraints. The constraints specifies a convex

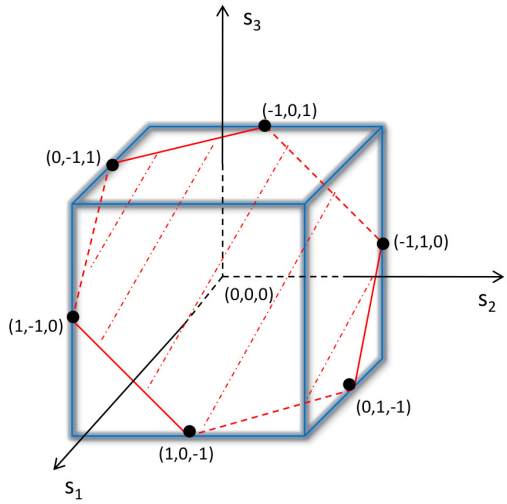

Figure 2: Polyhedral feasibility region for $M = 3$ electrodes. The blue cubic bounding box represents the maximum current constraints (9). This is intersected by the plane defined by the zero-sum current constraint (10). This results in the polyhedral feasibility region (shaded red). With a linear criterion possible solutions are found at the corner points (black dots).

feasibility region. To see this, note that the maximum current constraint (3) can be written equivalent as a constraint on each electrode, taking into account that the total current is zero:

$$-I_{max} \leq \mathbf{s} \leq I_{max}, \tag{9}$$

$$\mathbf{1s} = 0. \tag{10}$$

The $\leq$ sign in Eq. 9 is element-wise on $\mathbf{s}$. These boundaries are realized when the maximum current I_{max} enters and exits through a single electrode pair. Linear inequalities such as (9) & (10) specify a convex polyhedron. As an example, Figure 2 shows the polyhedron for $M = 3$ electrodes. With a linear optimality criterion this constitutes a linear programming problem (Grant et al., 2006). The fundamental theorem of linear programming states that the solutions are at the corner of the polyhedral feasibility region (black dots in Figure 2). Thus, to find the optimal solutions it suffices to check which corner gives the maximum intensity. The corners of our polyhedron correspond to current I_{max} passing through a single pair of electrodes. Say electrode i in vector $\mathbf{s}$ has current I_{max} and electrode j has current $-I_{max}$, with all other electrodes set to zero. All we have to do is to pick the pair of electrodes i, j that give the largest value for $\mathbf{e}^T\mathbf{As}$. If we define vector

$$\mathbf{v} = \mathbf{e}^T\mathbf{A}\,, \tag{11}$$

then i is simply the position with the largest value in vector $\mathbf{v}$, and j is the position with the smallest value. This solution has been first noted by Fernandez-Corazza et al. (2016, 2019).

Note that we could have also limited the current in each electrodes to lower values, say $-I_{max}/2 \leq \mathbf{s} \leq I_{max}/2$, while still limiting the total to $\mathbf{1s} \leq 2I_{max}$. This forces the total current to be split among at least two electrode pairs (four electrodes total). The purpose of this lower limit is to distribute currents over multiple locations and therefore reduce sensation while still injecting the same total current. We have done this in previous work and found the solutions

with numerical optimization (Dmochowski et al., 2013; Huang and Parra, 2019). Now we realize that these are still linear inequality constraints and thus result in a convex feasibility region. Thus, finding the optimal solution does not require any numerical optimization. The corners of this polyhedron have two electrodes passing current $+I_{max}/2$ and two electrodes passing $-I_{max}/2$. The maximum intensity on target will be achieved if we inject $+I_{max}/2$ though the two electrode locations with the largest values of $\mathbf{v}$ and draw $-I_{max}/2$ at the two locations with the smallest values of $\mathbf{v}$. Of course this argument applies not just for two pairs of electrodes, but any number of pairs.

Two comments may be in order about vector $\mathbf{v}$. First, if $\mathbf{e}$ represents a current source distribution in the brain, then the vector $\mathbf{v}$ is proportional to the voltage measured on the scalp by the same M electrodes. The origin of this connection is the reciprocity principle, first introduced for a single pair of electrodes by Rush and Driscoll (1969), and recently extended to arrays of electrodes by Dmochowski et al. (2017). Second, vector $\mathbf{v}$ and potentially matrix $\mathbf{Q}$ is really all that is needed for numerical optimization thus far.

2.4. Optimization of focality in interferential stimulation

To optimize interferential stimulation in terms of focality we add the constraint on the amplitude modulation at non-target locations. In analogy with (4) we constrain the square of modulation depth, summed over all locations in the non-target region:

$$||2\min(|\mathbf{\Gamma A s}_1|, |\mathbf{\Gamma A s}_2|)||^2 \leq P_{max}\,. \tag{12}$$

This is a non-convex constraint which complicates the numerical optimization. We solved optimization of the IFS criterion (5) s.t. (6) and (12) by sequential quadratic programming (SQP) (Brayton et al., 1979), which is implemented in the "`fminimax`" function in Matlab (R2016, MathWorks, Natick, MA).

2.5. Implementation details

To solve the convex optimization problems, such as for HD-TES (2 s.t. 3, 4) we use the CVX toolbox (Grant et al., 2006). This Matlab toolbox provides a high-level language interface where one can directly implement L1 norm constraints such as (3). Unfortunately it does not implement the minimum operation in (5). For this we introduce an auxiliary variable z and solve equivalently:

$$\begin{array}{ccc} \underset{\substack{\mathbf{s}_1,\mathbf{s}_2 \\ \mathbf{1s}_1=0,\mathbf{1s}_2=0}}{\arg\max} & 2\min(|\mathbf{vs}_1|,|\mathbf{vs}_2|) = & \underset{\substack{\mathbf{s}_1,\mathbf{s}_2,z \\ \mathbf{1s}_1=0,\mathbf{1s}_2=0 \\ z\leq\mathbf{vs}_1,z\leq\mathbf{vs}_2}}{\arg\max} \quad 2z \end{array} \tag{13}$$

To solve the non-convex optimization for IFS (5 s.t. 6, 12) we use the "`fminimax`" function in Matlab. This function allows one to directly implement the minimum operation in (5). Unfortunately it does not directly implementing the L1-norm constraint (6). Following the method proposed in (Tibshirani, 1996) we can formulate this constraint as set of simple linear constraints using auxiliary variables $\mathbf{s}^+$ and $\mathbf{s}^-$, which substitute for variable $\mathbf{s}$:

$$\mathbf{1}|\mathbf{s}| = \mathbf{1s}^+ + \mathbf{1s}^- \leq 2I_{max}, \tag{14}$$

$$\mathbf{s} = \mathbf{s}^+ - \mathbf{s}^-, \tag{15}$$

$$0 \leq \mathbf{s}^+, 0 \leq \mathbf{s}^-. \tag{16}$$

When adjusting the power constraint P_{max} at non-target area, we first calculate a default value of P_{max} as $\mathbf{e}^T\mathbf{A}(\mathbf{A}^T\mathbf{\Gamma}^2\mathbf{A})^{-1}\mathbf{A}^T\mathbf{e}$, which is the value that makes the criterion equivalent to least-squares criterion for maximum-focality (Fernandez-Corazza et al., 2019). We then vary this value across 12 different orders of magnitude, i.e., from $P_{max} \times 10^{-3}$ to $P_{max} \times 10^{8}$. When solving the IFS (5 s.t. 6, 12) for the first value of power constraint (i.e., $P_{max} \times 10^{-3}$), we initialize the "`fminimax`" function using the solution from HD-TES under the same power constraint. Then as the power constraint increases (relaxes), each solving for the IFS is initialized by the previous solution. For each value of P_{max}, the modulation depth / intensity and focality of the optimized electric field at the target location are computed. The focality is defined as the cubic-root of the brain volume with electric field modulation depth / intensity of at least 50% of the field intensity at the target (Huang and Parra, 2019).

2.6. Construction of the head model

The forward model **A** in this work was built on the ICBM152 (v6) template from the Montreal Neurological Institute (MNI, Montreal, Canada) (Mazziotta et al., 2001; Grabner et al., 2006)), following previously published routine (Huang et al., 2013). Briefly, the ICBM152 (v6) template MRI (magnetic resonance image) was segmented by the New Segment toolbox (Ashburner and Friston, 2005) in Statistical Parametric Mapping 8 (SPM8, Wellcome Trust Centre for Neuroimaging, London, UK) implemented in Matlab. Segmentation errors such as discontinuities in CSF and noisy voxels were corrected first by a customized Matlab script (Huang et al., 2013) and then by hand in an interactive segmentation software ScanIP (v4.2, Simpleware Ltd, Exeter, UK). Since tDCS modeling work has demonstrated the need to include the entire head down to the neck for realistic current flow, in particular in deep-brain areas and the brainstem (Huang et al., 2013), the field of view (FOV) of the ICBM152 (v6) MRI was extended down to the neck by registering and reslicing the standard head published in (Huang et al., 2013) to the voxel space of ICBM152 (see (Huang et al., 2016) for details). HD electrodes following the convention of the standard 10–10 international system (Klem et al., 1999) were placed on the scalp surface by custom Matlab script (Huang et al., 2013). Two rows of electrodes below the ears and four additional electrodes around the neck were also placed to allow for targeting of deeper cortical areas and for the use of distant reference electrodes in tDCS. A total of 93 electrodes were placed. A finite element model (FEM, (Logan, 2007)) was generated from the segmentation data by the ScanFE module in ScanIP. Laplace's equation was then solved (Griffiths, 1999) in Abaqus 6.11 (SIMULIA, Providence, RI) for the electric field distribution in the head. With one fixed reference electrode Iz as cathode, the electric field was solved for all other 92 electrodes with unit current density injected for each of them, giving 92 solutions for electric field distribution representing the forward model of the ICBM152 head, i.e., the matrix **A**. Note this matrix **A** is also the transpose of the EEG lead field **L** (Dmochowski et al., 2017). This data will be released upon publication.

3. Results

3.1. Effect of power constraint in non-target areas

The method proposed here maximizes the modulation depth at the target while constraining the power in non-target areas (see Section 2.1, 2.2, and 2.4). We first performed numerical experiments to study how the power constraint affects the optimization results for both HD-TES and IFS. Specifically, we numerically solved for the HD-TES criterion (2 s.t. 3, 4) and the IFS

criterion (5 s.t. 6, 12). The desired field direction **e** was selected to point in radial-in direction, and we varied the maximum allowable off-target power P_{max}. We computed the modulation depth / intensity and focality of the optimized electric field at the target location for each value of P_{max} (see Section 2.5 for details). This was done for four different target locations in the brain: 2 on the cortical surface and 2 in the deep brain region, with results shown in Figure 3. The first column shows the target locations in the axial MRI slice.

Following the common safety standard, total current was selected to not exceed 2 mA (or an L1-norm of 4 mA). For IFS, this is 1 mA for each of the two frequencies. For small values of P_{max} the total currents do not reach this allowable maximum, indicating that the power constraint dominates (Figure 3, second column, left of square markers). When power constraint is relaxed beyond this threshold values, then the full current is used. As we had predicted based on theoretical grounds (in Section 2.1), P_{max} regulates the trade-off between intensity and focality. Generally, as the power constraint in the non-target region is relaxed, modulation depth increases and focality deteriorates (area of stimulation increases in size). Figure 3 (third column, right of square markers) shows this trend for both IFS and HD-TES. Note for IFS, modulation depth is different from the intensity (Figure 1), while these two are the same for HD-TES. Evidently, for the same modulation depth at the target, the optimized IFS gives higher focality compared to optimized HD-TES in most instances (red vs. blue curves in Figure 3, third column). The intensity at the target from optimized IFS (orange curves in Figure 3, third column) does not show any advantage in terms of focality compared to IFS modulation depth or even HD-TES. It is also evident that these curves do not change monotonically with chaining P_{max}, which we ascribe the non-convex optimization criteria so that the result depends on initialization of the optimization.

3.2. Numerical solutions on a few examples

For the first two target locations in Figure 3 we fix P_{max} to the threshold value (square points in Figure 3 where current is fully utilized without losing focality). The resulting optimized modulation depth and field intensity are shown in Figure 4 and Figure 5 The two montages in panels B1 and B2 correspond to the currents $\mathbf{s}_1$ and $\mathbf{s}_2$ with the two different frequencies, injected through the same array. Note for IFS, modulation depth is different from the intensity, as shown in panels B3 and B4, respectively. Evidently, the intensity of the electric field from IFS totally missed the target locations, while the modulation depth from IFS achieves a focality that is about twice as high as that from HD-TES (1.16 cm vs. 2.82 cm at the cortical target, Figure 4; 4.21 cm vs. 7.84 cm at the deep target, Figure 5; all comparison under similar levels of modulation depth).

When the power constraint P_{max} (4 for HD-TES, 12 for IFS) is removed, we have the max-intensity solution for one location as shown in Figure 6 for HD-TES (panel A) and and IFS (panel B). As predicted mathematically (Section 2.2), one needs to inject the two frequencies at the same pair of electrodes, and the location of these two electrodes can be simply determined from the conventional HD-TES max-intensity solution (which is here confirmed numerically). The resulting modulation depth in radial direction (panel B3) is exactly the same as the electric field along the same direction induced by the HD-TES (panel A2). Therefore, in terms of intensity on target, IFS can not be any stronger than conventional HD-TES, even when optimizing electrode placement, but IFS does gain focality in modulation depth when optimized.

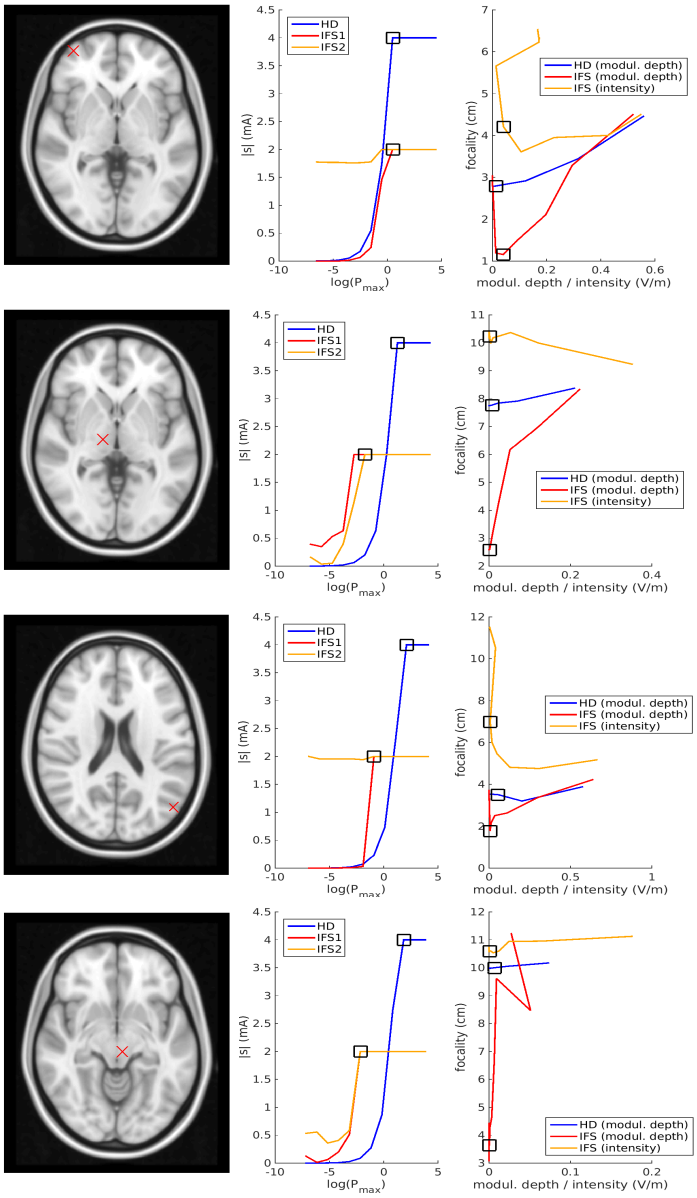

Figure 3: Modulation depth / Intensity and focality of optimized electric field along the radial direction at the target location for varying power constraints at non-target area, for both HD-TES and IFS. Results are shown for 4 target locations indicated by the red X in the MRI, with 2 on the cortical surface (1st and 3rd row), and 2 in the deep brain (2nd and 4th row). Total injected current intensity ($|\mathbf{s}|$) as the function of the power constraint P_{max} (on a logarithmic scale) is shown in the middle column (IFS1, IFS2: the two frequencies of IFS), with the black squares indicating the location where the full budget of injected current (4 mA) is used. Intensity-focality trade-off at different values of P_{max} (right column), with squares indicating injected current reaches the safety limit. Note for IFS, both modulation depth and intensity are shown.

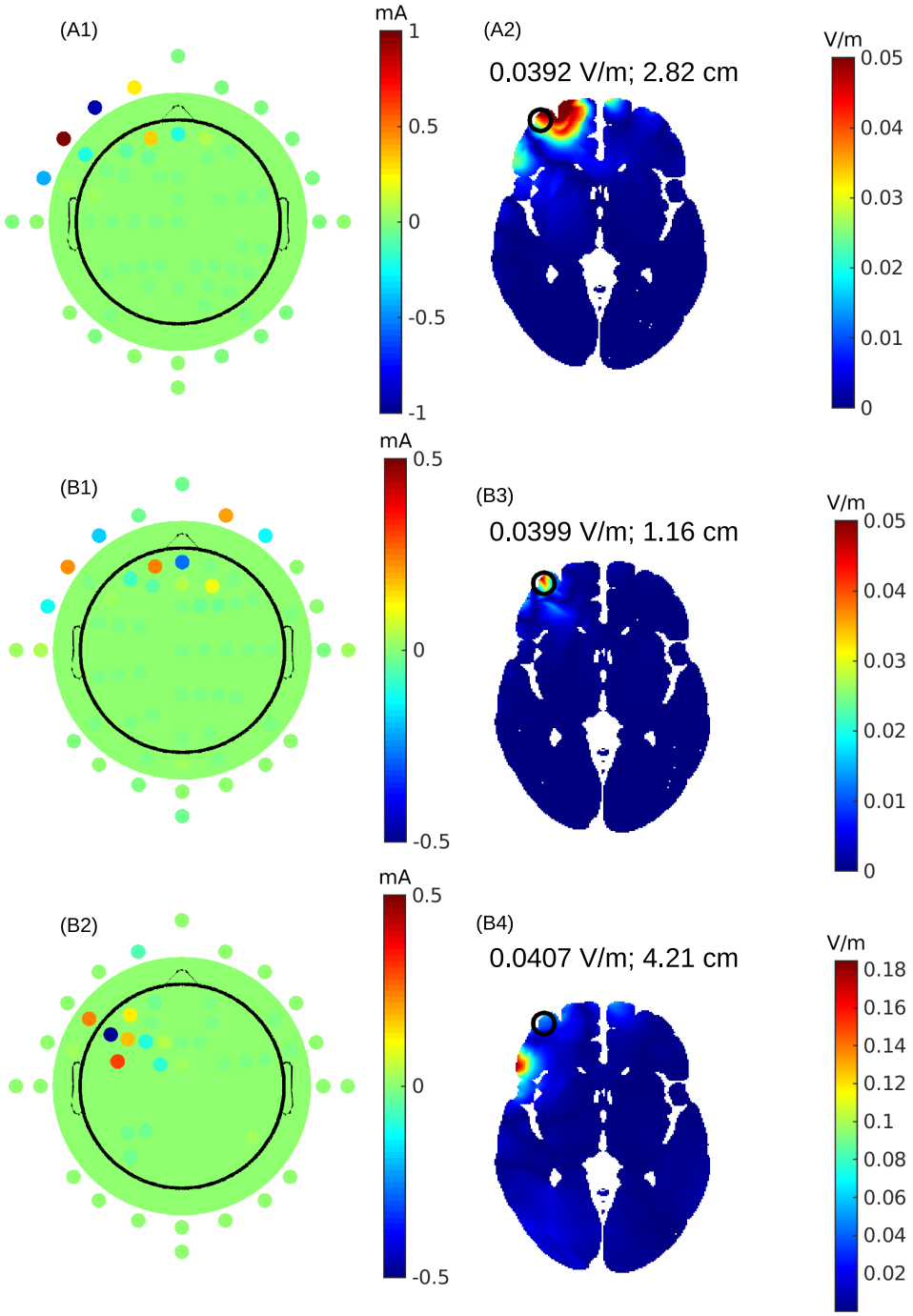

Figure 4: Solutions of maximizing the focality for conventional HD-TES (panel A) and IFS (panel B). Radial component of the modulation depth is shown for HD-TES (panel A2) and IFS (panel B3). The intensity of electric field is also shown for IFS (panel B4). The target is located at the cortical surface (black circles) and desired field points in radial direction. Modulation depth / intensity and focality are noted for the target location.

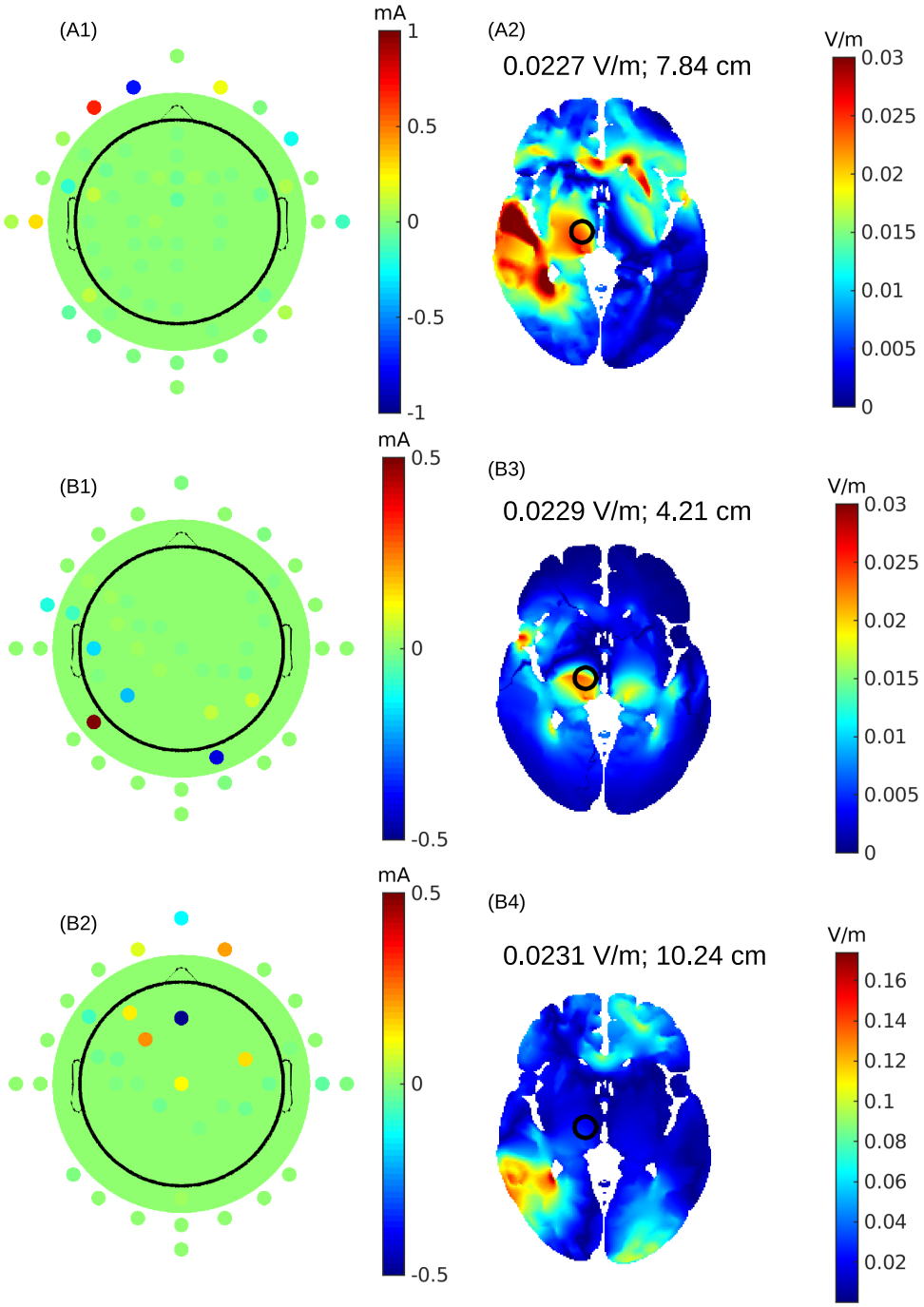

Figure 5: Same as Figure 4 but for a deep target (black circles).

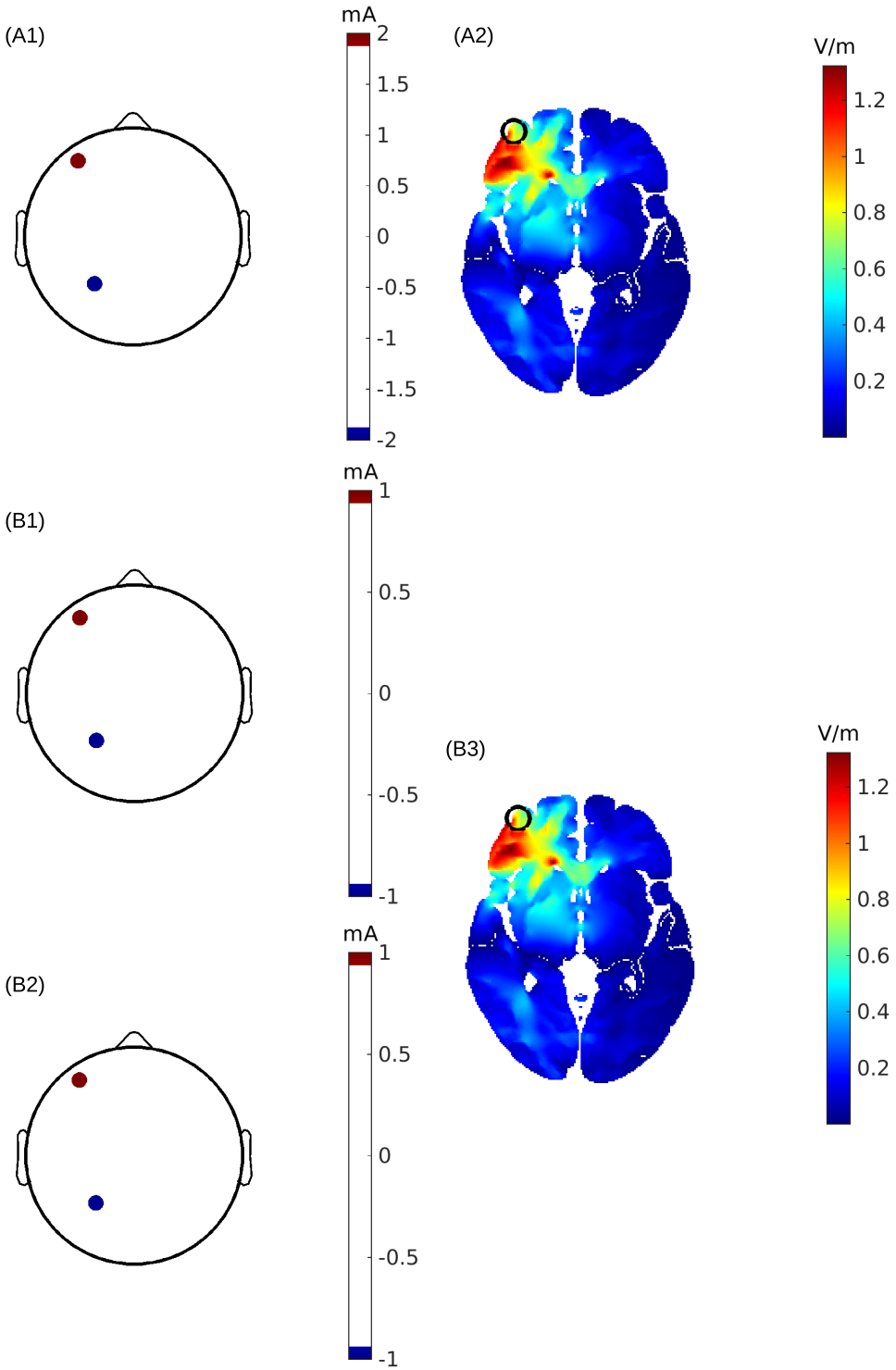

Figure 6: Numerical solutions of maximizing the electric field on the radial direction for conventional HD-TES (panel A) and interferential stimulation (panel B). The target location is indicated by a black circle in panels A2 and B3, where the radial component of the modulation depth is shown.

4. Discussion and Conclusions

In this work we addressed the optimization of IFS by considering an array of electrodes that can apply sinusoidal currents at two different frequencies. Each electrode can apply different current intensities for each frequency. This is significantly more flexible than recent optimization efforts for IFS that have been limited to pairs of electrodes of a single frequency each(Rampersad et al., 2019; Cao and Grover, 2019; Xiao et al., 2019). The approach can be readily implemented with existing multi-channel TES hardware by connecting the two current sources (of different frequency) to a single set of electrodes.

We found that maximizing the modulation depth of IFS results in a solution that "fuses" the two frequencies, in the sense that they are to be applied with the same intensity in a given electrode. The IFS solution is then equivalent to HD-TES with a modulated waveform (with 100% modulation). We further prove that this max-intensity montage – which is optimal for both HD-TES and IFS – can be found directly from the forward model.

We previously established for HD-TES that there is a fundamental trade-off between focality of and intensity of stimulation (Dmochowski et al., 2011). We find this trade-off here reproducible for the modulation depth of IFS. We leverage the optimization criterion of Guler et al. (2016) which allows one to titrate between the two extremes by constraining the power of stimulation in non-target areas: a tighter constraint make the result more focal, a looser constraint makes the stimulation modulation depth / intensity on target larger. When applying the same optimization criterion to the modulation depth of IFS we obtain a genuinely different optimization problem. The upside is that we find more focal stimulation for IFS as compared to HD-TES for otherwise similar modulation depth. This is true for cortical locations as well as deep brain areas. This appears to conflict with our previous conclusion on this topic (Huang and Parra, 2019), where we show that the two techniques were largely the same in terms of focality. One caveat of that earlier work is that the electrode arrays had not been systematically optimized, and thus we left the possibility open that IFS could be more focal than HD-TES. Here we conclude that this is in fact the case once currents through each electrode have been systematically optimized.

When designing stimulation montages, what should one focus on, intensity of the high frequency carrier, or its modulation depth? For HD-TES they can be readily made the same (Figure 1). For IFS they are not, and in fact as we shown in Figures 4 and 5 they can be quite different. The premise of IFS is that high frequencies have no effect on nervous tissue, and instead, neurons and/or nerve fivers respond more readily to the modulation or transients of the high-frequency stimulation (Grossman et al., 2017). Thus, it may make sense to focus on modulation depth instead of intensity. However, empirical validation of this assumption is mixed (unpublished data). Therefore, while optimization of IFS has focused on the modulation depth here, we also report the associated intensities of the high frequency carrier.

The advantage in focality of IFS comes from the *min*() operation in calculating the modulation depth (Eq. 12). This operation is element-wise and it goes through all the locations in the non-target area, which makes it computationally very expensive (optimization with the "fminmax" function take 1–2 hours on a standard PC). Additionally, the optimization criterion becomes non-convex, which causes sub-optimal solutions if the search is not properly initialized. (We believe that this is the source of the non-monotonic relationship between focality and intensity observed in Figure 3.) We have tested alternative criteria but find in all instances that the optimal solutions again "fuse" the two frequencies (see Appendix). In other words, without the location-wise *min*() operation we have not been able to achieve any different solution than the conventional HD-TES. The *min*() operation appears to break the symmetry of the solution leading to higher focality

compared to HD-TES.

In conclusion, the naive approaches advocated for IFS so far do not meaningfully outperform HD-TES. Yet, here we provide a proof-of-principle that more focal stimulation is possible with IFS. The challenge remains to find an efficient convex optimization criterion that can exploit the full potential of IFS for the purpose of focal non-invasive deep brain stimulation.

ACKNOWLEDGMENT

This work was supported by the NIH Grants R01MH111896, R44NS092144, R01NS095123, and by Soterix Medical Inc.

References

Ashburner, J., Friston, K. J., Jul. 2005. Unified segmentation. NeuroImage 26 (3), 839–851.

Bikson, M., Bulow, P., Stiller, J., Datta, A., Battaglia, F., Karnup, S., Postolache, T., 2008. Transcranial direct current stimulation for major depression: A general system for quantifying transcranial electrotherapy dosage. Current Treatment Options in Neurology 10 (5), 377–385.

Brayton, R., Director, S., Hachtel, G., Vidigal, L., Sep. 1979. A new algorithm for statistical circuit design based on quasi-newton methods and function splitting. IEEE Transactions on Circuits and Systems 26 (9), 784–794.

Cao, J., Grover, P., 2019. Stimulus: Noninvasive dynamic patterns of neurostimulation using spatio-temporal interference. IEEE Transactions on Biomedical Engineering, 1–1.

Datta, A., Bansal, V., Diaz, J., Patel, J., Reato, D., Bikson, M., Oct. 2009. Gyri-precise head model of transcranial DC stimulation: Improved spatial focality using a ring electrode versus conventional rectangular pad. Brain stimulation 2 (4), 201–207.

Dmochowski, J., Bikson, M., 2017. Noninvasive neuromodulation goes deep. Cell 169 (6), 977–978.

Dmochowski, J. P., Datta, A., Bikson, M., Su, Y., Parra, L. C., Aug. 2011. Optimized multi-electrode stimulation increases focality and intensity at target. Journal of Neural Engineering 8 (4), 046011.

Dmochowski, J. P., Datta, A., Huang, Y., Richardson, J. D., Bikson, M., Fridriksson, J., Parra, L. C., Jul. 2013. Targeted transcranial direct current stimulation for rehabilitation after stroke. NeuroImage 75, 12–19.

Dmochowski, J. P., Koessler, L., Norcia, A. M., Bikson, M., Parra, L. C., 2017. Optimal use of eeg recordings to target active brain areas with transcranial electrical stimulation. NeuroImage.

Edwards, D., Cortes, M., Datta, A., Minhas, P., Wassermann, E. M., Bikson, M., Jul. 2013. Physiological and modeling evidence for focal transcranial electrical brain stimulation in humans: A basis for high-definition tDCS. NeuroImage 74, 266–275.

Fernandez-Corazza, M., Turovets, S., Luu, P., Anderson, E., Tucker, D., 2016. Transcranial electrical neuromodulation based on the reciprocity principle. Frontiers in psychiatry 7, 87.

Fernandez-Corazza, M., Turovets, S., Muravchik, C. H., 2019. Unification of optimal targeting methods in transcranial electrical stimulation. bioRxiv.
URL `https://www.biorxiv.org/content/early/2019/02/21/557090`

Fregni, F., Gimenes, R., Valle, A. C., Ferreira, M. J. L., Rocha, R. R., Natalle, L., Bravo, R., Rigonatti, S. P., Freedman, S. D., Nitsche, M. A., PascualLeone, A., Boggio, P. S., Dec. 2006. A randomized, sham-controlled, proof of principle study of transcranial direct current stimulation for the treatment of pain in fibromyalgia. Arthritis & Rheumatism 54 (12), 3988–3998.

Gembicki, F., Haimes, Y., December 1975. Approach to performance and sensitivity multiobjective optimization: The goal attainment method. IEEE Transactions on Automatic Control 20 (6), 769–771.

Goats, G., 1990. Interferential current therapy. British journal of sports medicine 24 (2), 87.

Grabner, G., Janke, A. L., Budge, M. M., Smith, D., Pruessner, J., Collins, D. L., 2006. Symmetric atlasing and model based segmentation: an application to the hippocampus in older adults. Medical image computing and computer-assisted intervention: MICCAI: International Conference on Medical Image Computing and Computer-Assisted Intervention 9 (Pt 2), 58–66.

Grant, M., Boyd, S., Ye, Y., 2006. Disciplined Convex Programming. In: Liberti, L., Maculan, N. (Eds.), Global Optimization: From Theory to Implementation. Nonconvex Optimization and Its Applications. Springer US, Boston, MA, pp. 155–210.
URL `https://doi.org/10.1007/0-387-30528-9_7`

Griffiths, D. J., 1999. Introduction to electrodynamics, 3rd Edition. Prentice Hall, Upper Saddle River, NJ.

Grossman, N., Bono, D., Dedic, N., Kodandaramaiah, S. B., Rudenko, A., Suk, H.-J., Cassara, A. M., Neufeld, E., Kuster, N., Tsai, L.-H., et al., 2017. Noninvasive deep brain stimulation via temporally interfering electric fields. Cell 169 (6), 1029–1041.

Guler, S., Dannhauer, M., Erem, B., Macleod, R., Tucker, D., Turovets, S., Luu, P., Erdogmus, D., Brooks, D. H., Jun. 2016. Optimization of focality and direction in dense electrode array transcranial direct current stimulation (tDCS). Journal of Neural Engineering 13 (3), 036020.

Huang, Y., Dmochowski, J. P., Su, Y., Datta, A., Rorden, C., Parra, L. C., Dec. 2013. Automated MRI segmentation for individualized modeling of current flow in the human head. Journal of Neural Engineering 10 (6), 066004.

Huang, Y., Parra, L. C., 2019. Can transcranial electric stimulation with multiple electrodes reach deep targets? Brain Stimulation 12 (1), 30 – 40.

Huang, Y., Parra, L. C., Haufe, S., 2016. The new york head – a precise standardized volume conductor model for eeg source localization and tes targeting. NeuroImage 140, 150 – 162.

Klem, G. H., Lders, H. O., Jasper, H. H., Elger, C., 1999. The ten-twenty electrode system of the international federation. the international federation of clinical neurophysiology. Electroencephalography and clinical neurophysiology. Supplement 52, 3–6.

Logan, D. L., 2007. A First Course in the Finite Element Method, 4th Edition. Nelson, Toronto.

Mazziotta, J., Toga, A., Evans, A., Fox, P., Lancaster, J., Zilles, K., Woods, R., Paus, T., Simpson, G., Pike, B., Holmes, C., Collins, L., Thompson, P., MacDonald, D., Iacoboni, M., Schormann, T., Amunts, K., Palomero-Gallagher, N., Geyer, S., Parsons, L., Narr, K., Kabani, N., Le Goualher, G., Feidler, J., Smith, K., Boomsma, D., Pol, H. H., Cannon, T., Kawashima, R., Mazoyer, B., 2001. A four-dimensional probabilistic atlas of the human brain. Journal of the American Medical Informatics Association : JAMIA 8 (5), 401–430.

Nitsche, M. A., Paulus, W., Sep. 2000. Excitability changes induced in the human motor cortex by weak transcranial direct current stimulation. The Journal of Physiology 527 (3), 633–639.

Nitsche, M. A., Schauenburg, A., Lang, N., Liebetanz, D., Exner, C., Paulus, W., Tergau, F., 2003. Facilitation of implicit motor learning by weak transcranial direct current stimulation of the primary motor cortex in the human. Journal of Cognitive Neuroscience 15 (4), 619–626.

Rampersad, S., Roig-Solvas, B., Yarossi, M., Kulkarni, P. P., Santarnecchi, E., Dorval, A. D., Brooks, D. H., 2019. Prospects for transcranial temporal interference stimulation in humans: a computational study. bioRxiv.
URL `https://www.biorxiv.org/content/early/2019/06/19/602102`

Rush, S., Driscoll, D. A., Jan. 1969. EEG electrode sensitivity–an application of reciprocity. IEEE transactions on biomedical engineering 16 (1), 15–22.

Schlaug, G., Renga, V., Nair, D., Dec. 2008. Transcranial direct current stimulation in stroke recovery. Arch Neurol 65 (12), 1571–1576.

Shen, H., February 2018. Brain stimulation is all the rage–but it may not stimulate the brain.

Tibshirani, R., 1996. Regression Shrinkage and Selection via the Lasso. Journal of the Royal Statistical Society. Series B (Methodological) 58 (1), 267–288.
URL `https://www.jstor.org/stable/2346178`

Xiao, Q., Zhong, Z., Lai, X., Qin, H., 06 2019. A multiple modulation synthesis method with high spatial resolution for noninvasive neurostimulation. PLOS ONE 14 (6), 1–15.
URL `https://doi.org/10.1371/journal.pone.0218293`

Appendix

As an alternative to Eq. (12), one could limit an upper bound of the power, by exploiting the relationships: $\|\min(|\mathbf{E}_1|, |\mathbf{E}_2|)\|^2 \leq \|\mathbf{E}_1\|^2 + \|\mathbf{E}_2\|^2$. With this we could limit the total power summed over off-target locations:

$$\|\min(|\mathbf{\Gamma A s}_1|, |\mathbf{\Gamma A s}_2|)\|^2 \leq \|\mathbf{\Gamma A s}_1\|^2 + \|\mathbf{\Gamma A s}_2\|^2 \leq P_{max} \tag{17}$$

Alternatively, based on the upper bound (7), we could limit the amplitude at off-target locations:

$$\min(|\mathbf{\Gamma A s}_1|, |\mathbf{\Gamma A s}_2|) \leq |\mathbf{\Gamma A s}_1| + |\mathbf{\Gamma A s}_2| \leq M_{max} \tag{18}$$

Both constraints (17) and (18) are convex so that the optimization of the linear criterion (2) subject to these constraints can be solved efficiently with established convex optimization tools (Section 2.5). We found numerically for both these constraints that the optimum is again given by the symmetric solution, $\mathbf{s} = \mathbf{s}_1 = \mathbf{s}_2$, as in the max-intensity solution (Eq. 8).